Molecular Biology of the Cell
Vol. 15, 4658–4668, October 2004

Visualization of Regulated Exocytosis with a Granule-Membrane Probe Using Total Internal Reflection Microscopy[V]

Miriam W. Allersma,* Li Wang,† Daniel Axelrod,* and Ronald W. Holz†‡

Departments of †Pharmacology and *Physics and Biophysics Research Division, University of Michigan, Ann Arbor, MI 48109

Submitted February 23, 2004; Revised July 15, 2004; Accepted July 20, 2004
Monitoring Editor: Jennifer Lippincott-Schwartz

Secretory granules labeled with Vamp-green fluorescent protein (GFP) showed distinct signatures upon exocytosis when viewed by total internal reflection fluorescence microscopy. In ~90% of fusion events, we observed a large increase in fluorescence intensity coupled with a transition from a small punctate appearance to a larger, spreading cloud with free diffusion of the Vamp-GFP into the plasma membrane. Quantitation suggests that these events reflect the progression of an initially fused and spherical granule flattening into the plane of the plasma membrane as the Vamp-GFP simultaneously diffuses through the fusion junction. Approximately 10% of the events showed a transition from puncta to ring-like structures coupled with little or no spreading. The ring-like images correspond quantitatively to granules fusing and retaining concavity (recess of ~200 nm). A majority of fusion events involved granules that were present in the evanescent field for at least 12 s. However, ~20% of the events involved granules that were present in the evanescent field for no more than 0.3 s, indicating that the interaction of the granule with the plasma membrane that leads to exocytosis can occur within that time. In addition, ~10% of the exocytotic sites were much more likely to occur within a granule diameter of a previous event than can be accounted for by chance, suggestive of sequential (piggy-back) exocytosis that has been observed in other cells. Overall granule behavior before and during fusion is strikingly similar to exocytosis previously described in the constitutive secretory pathway.

INTRODUCTION

The late steps in the regulated, secretory pathway are complex. High temporal resolution electrophysiological studies suggest that there are interconnected pools of secretory granules close to the plasma membrane with different characteristic rates of exocytosis (Voets, 2000; Rettig and Neher, 2002). The final fusion event itself is regulated and occurs in steps (Breckenridge and Almers, 1987; Zimmerberg *et al*., 1987). The first evidence of fusion is the formation of a short-lived, relatively low-conductance fusion pore, which is permeant to low-molecular-weight contents such as catecholamine (in chromaffin cells). This is usually followed by a rapidly expanding pore that results in full content release (Albillos *et al*., 1997; Dernick *et al*., 2003).

Investigation of the final events in the secretory pathway has been aided by real-time imaging of secretory granules in resting and stimulated cells by total internal reflection fluorescence microscopy (TIRFM), which is used in the present study. TIRFM selectively illuminates the aqueous phase immediately adjacent to a glass interface with an exponentially decaying excitation (decay constant of 50–100 nm). The theoretical basis and practical implementation of the technique have been well described (Axelrod, 1981, 2001, 2003; Stout and Axelrod, 1989). In most studies, the lumenal contents of secretory granules have been labeled with fluorescent weak bases such as acridine orange (Steyer *et al*., 1997; Oheim *et al*., 1998; Oheim and Stuhmer, 2000) (labels all acidic organelles) or green fluorescent protein (GFP)-tagged proteins that are sorted to the secretory granule (Burke *et al*., 1997; Han *et al*., 1999; Johns *et al*., 2001; Ohara-Imaizumi *et al*., 2002). A common finding is that secretory granules in neuroendocrine cells are for the most part highly restricted in their motion, possibly because of interaction with the subplasma membrane cytoskeleton. The rapid disappearance of granule contents and the occasionally captured cloud of fluorescence in the extracellular medium demonstrates that these fluorescent, membrane-proximal granules are able undergo exocytosis (Steyer *et al*., 1997; Oheim *et al*., 1998; Ng *et al*., 2002; Ohara-Imaizumi *et al*., 2002; Duncan *et al*., 2003).

A primary goal in this study was the visualization and analysis of the fusion event from the point of view of a membrane protein that can diffuse from the granule to the plasma membrane upon fusion. This approach has been used previously in constitutive secretion (Schmoranzer *et al*., 2000; Toomre *et al*., 2000) and lysosome secretion (Jaiswal *et al*., 2002) but not in regulated secretion in neuroendocrine cells. Because diffusion of a membrane protein from the granule to the plasma membrane is likely to give a longer lasting signal of exocytosis than a rapidly released soluble granule constituent, fusion events should be easier to detect using a granule membrane protein marker. Importantly, the

Article published online ahead of print. Mol. Biol. Cell 10.1091/mbc.E04–02–0149. Article and publication date are available at www.molbiolcell.org/cgi/doi/10.1091/mbc.E04–02–0149.

[V] The online version of this article contains supplemental material accessible through http://www.molbiolcell.org.

‡ Corresponding author. E-mail address: holz@umich.edu.

Abbreviations used: DMPP, 1,1 dimethyl-4-phenylpiperzinium; GFP, green fluorescent protein; hGH, human growth hormone; PSS, physiological salt solution; TIRFM, total internal reflection fluorescence microscopy.

fluorescent changes of a granule membrane protein might provide new insights into the fusion event. We found that the v-SNARE, Vamp, with GFP fused to its C terminus (lumenal), was such a probe. Vamp-GFP was used to label secretory granules in chromaffin cells to study the dynamics of the fusion process and of the preceding granule motion.

MATERIALS AND METHODS

Cell Preparation and Experimental Setup

Chromaffin cell preparation, transient transfection, and plating onto collagen-coated coverslips (1.78 refractive index) were performed as described previously (Wick *et al*., 1993; Wilson *et al*., 1996; Johns *et al*., 2001). Experiments were performed 4–8 d after culture preparation in a physiological salt solution (PSS) containing 145 mM NaCl, 5.6 mM KCl, 2.2 mM $CaCl_2$, 0.5 mM $MgCl_2$, 15 mM HEPES, pH 7.4, and 5 mg/ml bovine serum albumin at ~22°C. Perfusion solution (PSS) was continuously delivered to individual cells through a 0.2-μm inner diameter quartz pipette under positive pressure. Cells were stimulated by switching the perfusion solution to PSS containing the nicotinic agonist 1,1 dimethyl-4-phenylpiperzinium (DMPP) (20 μM) for 3–5 s. Fusion events were apparent during or within 15 s after perfusion with DMPP. The mammalian expression vector for Vamp2 fused on the C terminus (lumenal) to enhanced green fluorescent protein (EGFP) was a gift from Dr. Richard Scheller (Stanford University, Stanford, CA, and Genentech, South San Francisco, CA).

Immunocytochemistry for Confocal Microscopy

Chromaffin cells were transiently cotransfected with plasmids encoding Vamp-GFP and human growth hormone (hGH). Cells were fixed, permeabilized with ice-cold methanol, and exogenous hGH or endogenous dopamine-β-hydroxylase were detected with rabbit primary antibodies and lissamine-tagged goat anti-rabbit goat secondary antibody as described previously (Wick *et al*., 1993). Quantitation of the colocalization was performed on cells that had good coexpression of hGH and Vamp-GFP. It was determined whether Vamp-GFP-expressing puncta colocalized with hGH. This was done in Adobe Photoshop where puncta in the overlapping image were queried for colocalization by turning off and on the green and red channels.

Total Internal Reflection Fluorescence Microscopy

Objective-based TIRFM was obtained by directing an Argon ion 488-nm laser (3W Lexel model 95) through a custom side port to a side-facing dichroic mirror Q495LPw/AR (Chroma Technology, Brattleboro, VT) and a HQ500 LP emission filter (Chroma Technology) on an IX70 (inverted) microscope (Olympus, Tokyo, Japan). The beam was focused on the periphery of the back focal plane of a 100× 1.65 numerical aperture (NA), oil immersion objective (Olympus) so that the laser beam was incident on the coverslip at 58.4–64.2° to the optical axis giving a decay constant of the evanescent field of 48–62 nm. Digital images were captured on a cooled charge-coupled device camera (SensiCam; Cooke, Auburn Hills, MI). Images were acquired at 10–14 Hz with exposure times of 20–50 ms.

Image Analysis

Granules were identified and tracked through a time-sequence stack of images by using software written by the authors in Interactive Data Language (IDL; Research Systems, Boulder, CO) with methods similar to those described previously (Johns *et al*., 2001). These procedures permitted the analysis of vast amounts of information. Granules undergoing exocytosis were visually identified. From the stack of images, a data set was generated containing x and y coordinates, granule intensity (background subtracted), and local background for each granule in each frame. The x and y coordinates were determined from band-pass–filtered images. Positions were calculated from the peaks of the parabolas determined by the intensities of the brightest pixel and each of the four immediately adjacent pixels. Total granule intensity was determined in unfiltered images from the total pixel intensity within a circular region (600 nm in diameter, 81 pixel area) around the granule center after the local background was subtracted. The local background was the average intensity of a ring of 32 pixels just outside the circle. The data set was then analyzed to track granules, calculate interframe motions, and determine other parameters as indicated in the results and in the figure legends.

The frame just before exocytosis, f_0, was identified as the frame before the occurrence of significant increases in fluorescence intensity or width (see below).

Analysis of the Spreading Fluorescence upon Fusion

The intensity profiles were created from a 27 × 27 pixel (1.62 × 1.62 μm) region of interest (ROI), including the granule and some of its surroundings. The large size was chosen so that it would include the cloud of fluorescence as it spread after fusion. The intensity was averaged as a function of radial distance, r, from the granule center. The width was calculated from a Gaussian fit to the radially averaged intensities.

The intensity of the Vamp-GFP as it spread in the plasma membrane was determined after background fluorescence was subtracted from the ROI. This background fluorescence was calculated by subtracting the intensity of the granule from the total intensity of the ROI in the frame just before fusion (f_0). In subsequent frames (in which Vamp-GFP had spread), this value was subtracted from the total fluorescence in the ROI to obtain the Vamp-GFP intensity from the fused granule.

Modeling of Fusion Events

The image pattern that would be expected with TIRFM optics during the course of fusion of a spherical granule with the planar plasma membrane was computed by a custom IDL program. The model assumed here had the following features.

First, a sphere of 150-nm outside equivalent radius and 144-nm inside equivalent radius is truncated by a plane representing the plasma membrane (Figure 6). The nontruncated region preserves its spherical shape and radius. The truncated area flattens to a planar circular ring with a central hole at the truncation and an outside radius such that the total surface area of the truncated sphere plus the planar circular ring conserves the surface area of the initial sphere. Second, the depth of the truncation is variable, such that the distance from the plane (at $z = 0$) to the distal point of the sphere is called the "actual" indentation depth z_{actual}. Third, the pixels representing this geometrical structure are assigned "intensity" values of $\exp(-z/d)$ where z is the (nanometer-equivalent) distance of the pixel to the plane and d is the evanescent field depth (assumed to be 55 nm). Fourth, the structure is projected onto a two-dimensional (2D) plane by summing all the pixel intensity values along z at each particular (x,y) coordinate. Fifth, the projected map is convoluted with an Airy disk function (representing the microscope point spread function for emission). The equivalent radius of the Airy disk (center to first minimum) is set at w = 184 nm, which is the theoretical value for a 1.65 NA objective at 500-nm wavelength. This width agrees with the experimentally observed value (obtained from images of 20-nm-diameter fluorescent beads; Molecular Probes, Eugene, OR) of 180–240 nm. These convoluted maps are depicted in Figure 6A for various actual indentation depths. Sixth, the intensity I_0 in the center of the convoluted maps is compared with the maximum intensity I_m in the map and converted to an "apparent" indentation depth by $z_{apparent} = d\ln(I_0/I_m)$. The relationship between z_{actual} and $z_{apparent}$ is shown in Figure 6B, f. Possible diffusion of fluorescent material at the periphery of the flattened ring is not included in the model, so the expected spreading depicted in Figure 6A may be an underestimate of its true extent. Possible distortion of the granule shape during fusion also is not modeled here. Unless otherwise indicated, data are presented as the mean ± SE.

RESULTS

Vamp-GFP Is a Membrane Marker of the Chromaffin Granule

Vamp-GFP colocalized almost exclusively with secretory granules (chromaffin granules) in bovine chromaffin cells. When cotransfected with hGH, a protein that trafficks to chromaffin granules (Wick *et al*., 1993), Vamp-GFP colocalized with hGH (Figure 1) with 73% of the Vamp-GFP–expressing granules also expressing hGH (1264 granules, 13 cells). In other experiments, 84% of the granules with Vamp-GFP (256 granules, 5 cells) also stained for the endogenous granule protein dopamine-β-hydroxylase. In most cells, there was little Vamp-GFP on the plasma membrane. In separate experiments, it was found that transiently expressed Vamp-GFP did not significantly alter the secretion of coexpressed hGH (unpublished data).

Distinct TIRFM Signal of Granule Fusion to Plasma Membrane

Punctate Vamp-GFP in chromaffin cells was readily visualized by TIRFM, indicating that the Vamp-GFP–labeled granules were located within several hundred nanometers of the plasma membrane. As expected from previous studies, motion of the granules in all three dimensions was evident but highly restricted with only a small fraction of the granules moving more than a granule diameter during 30 s of observation. Within seconds of stimulation with the nicotinic

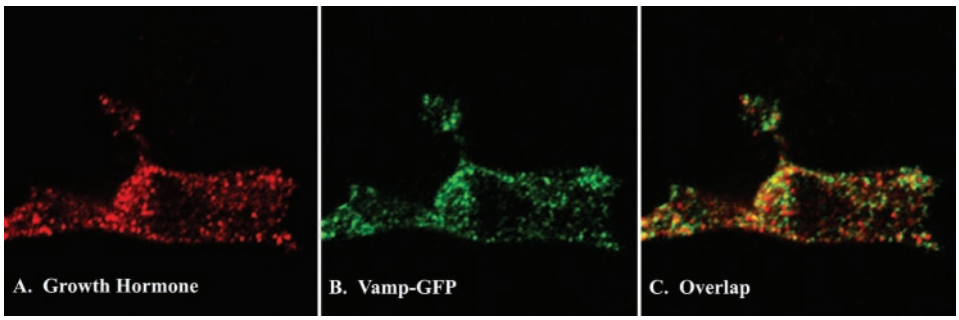

Figure 1. Vamp-GFP colocalizes with chromaffin granules in chromaffin cells. Chromaffin cells were cotransfected with plasmids encoding hGH and Vamp-GFP. Four days later, cells were fixed, permeabilized, and the hGH detected with immunocytochemistry by using anti-hGH. Transfected cells were visualized by confocal microscopy. (A) hGH. (B) Vamp-GFP (GFP fluorescence). (C) overlap (yellow).

agonist DMPP, the fluorescence of some granules quickly brightened and then spread (see Supplemental Movie 1). These were the most common events. They required extracellular Ca^{2+} and were never observed without stimulation. The spreading occurred over hundreds of milliseconds and was interpreted as Vamp-GFP diffusing from the chromaffin granule membrane into the plasma membrane, a conclusion that is fully supported by the analysis below.

The increase in the integrated intensity of granular Vamp-GFP fluorescence and the spreading of the fluorescence upon fusion were quantitated (Figure 2). The fluorescence intensity greatly increased in the first 0.1 s upon fusion. The radial distribution of pixel intensities is shown below the images. The fluorescence spread evenly and almost completely disappeared into the background by 1 s. In 90% of the fusion events, the center pixels were the brightest at all times after fusion. Sometimes a small amount of Vamp-GFP remained punctate after the initial spreading. This residual fluorescence could represent punctate Vamp-GFP in the plasma membrane or the capture of fused granule membrane by rapidly formed endocytic vesicles.

The bright center and spreading fluorescence was further analyzed. The spread of the Vamp-GFP fluorescence before and during spreading was measured as the width of a Gaussian distribution that best fit the radial distribution of pixel intensities. The integrated intensities of the Vamp-GFP from granules before and after fusion were determined. Quantitative descriptions of the events could be obtained in 37 events. In 26 events (70%), the initial fluorescence increase occurred simultaneously with the spreading of Vamp-GFP fluorescence (Figure 3, event 148); in 10 events (27%), the initial increase preceded the spreading (Figure 3, event 48). In only one event did the widening seem to occur before the increased fluorescence.

The increased fluorescence intensity upon fusion was expected for several reasons. First, the granule may be moving closer to the plasma membrane and thus closer to the coverslip into a brighter region of the evanescent field. Second, when the granule lumen opens to the extracellular medium, the pH jumps from 5.5 to 7.4. The GFP that was fused to Vamp is pH sensitive. In experiments with fixed and Triton X-100–permeabilized cells, we found that such a pH jump increased the EGFP fluorescence by a factor of 1.7 (unpublished data). Third, the Vamp-GFP would be brought closer to the glass interface upon fusion by diffusion of the protein from the granule membrane into the plasma membrane and/or flattening of the granule membrane into the plasma membrane. For a chromaffin granule (300 nm in diameter), complete deposition of granule Vamp-GFP into the plasma membrane will increase fluorescence five- to sixfold (Schmoranzer *et al*., 2000). Altogether, the increase in total granule fluorescence would be predicted to be eight to 10-fold, or somewhat greater if the granule moves toward the plasma membrane in the last 100 ms before fusion. The actual increase was 8.9 ± 1.0-fold (n = 42) in good agreement with the predicted increase. The range was 3- to 27-fold (Figure 5B, bright center, spreading). The large range of values probably reflects variability in granule size, intragranular pH, distance of the granule from the plasma membrane in

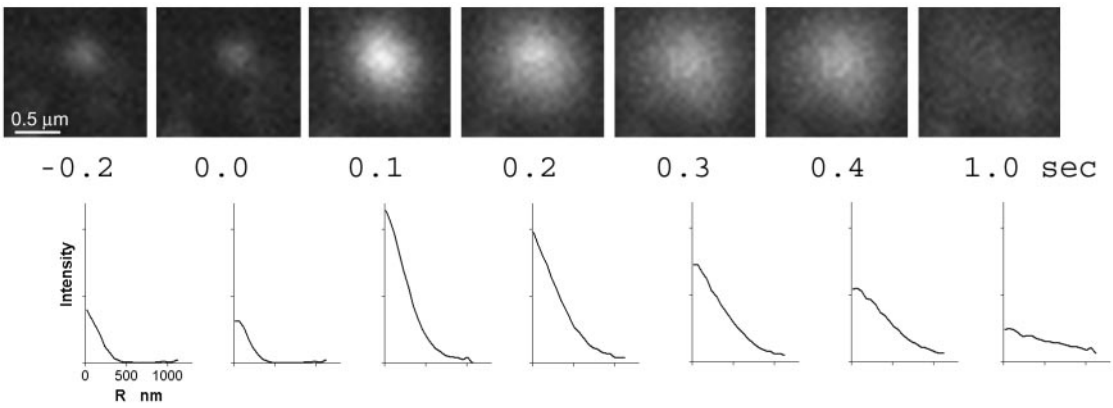

Figure 2. An intensity burst characterizes the fusion of an individual Vamp-GFP-labeled granule with the plasma membrane. Successive frames show the fusion of a Vamp-GFP–containing granule and the subsequent spread of the Vamp-GFP in the plasma membrane. The frame just before fusion is t = 0.0 s. Below each image is the Vamp-GFP intensity (with background subtracted) averaged as a function of radial distance (*r*) away from the granule center. Note that peak intensity is in the center of the intensity profile at all times. The fluorescence almost completely disappeared after 1 s.

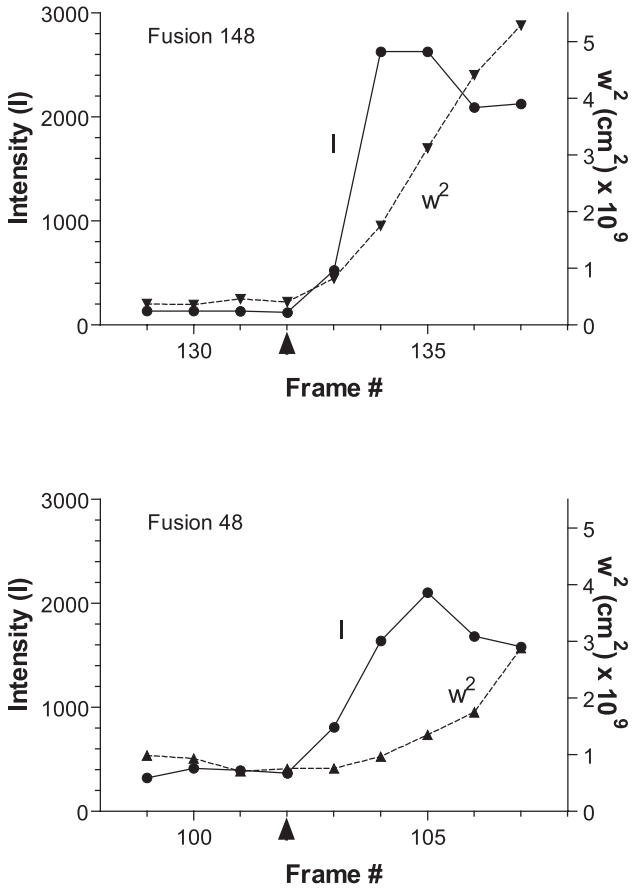

Figure 3. Analysis of the total intensity and width of the fluorescence profile. The total intensity I of Vamp-GFP from individual granules and the width squared, w^2, of the radially averaged Gaussian fit of the intensity profile in each frame before, during, and after fusion were determined. Two events are shown. In fusion 148, the total intensity and the w^2 increased simultaneously. In fusion 48, the total intensity rose before w^2 increased significantly. The arrowhead along the x-axis indicates the frame immediately preceding fusion. The frame rate was 10 Hz.

the frame before exocytosis, and the degree of granule membrane flattening (see below).

One of the first consequences of formation of the fusion pore is an increase of the granule interior pH and a resulting increase in GFP fluorescence. Indeed, the increase in intensity almost always occurred either simultaneously with or preceding the spreading of the fluorescence in the plasma membrane with images. In 40% of the events that could be quantitated, the fluorescence increase was maximal within one frame (100 ms), which is within the time scale of fusion events measured electrophysiologically (Albillos *et al*., 1997; Dernick *et al*., 2003). This fraction is an underestimate because it is likely that some fusion events began during the capture of the image. Seventy-nine percent were maximal within 200 ms.

Diffusion of Vamp-GFP after Fusion

In those 90% of the events in which Vamp-GFP spread rapidly in the plane of the plasma membrane, the width doubled in 0.27 ± 0.02 s (n = 23). The diffusion coefficient, D, of the Vamp-GFP in the plasma membrane for the above-mentioned events was calculated from the slope the plot of w^2 versus time by using $D = \Delta w^2/4\Delta t$, where w^2 (width squared) is the variance of the Gaussian fit of the GFP fluorescence in an image. A mean diffusion coefficient of $2.0 \pm 0.3 \times 10^{-9}$ cm^2/s was calculated for 13 events with approximately linear increases in w^2 with time.

Fusion Events in Which the Center Has a Lower Fluorescence than the Surround

Approximately 10% of the events observed upon nicotinic stimulation were qualitatively different from the bright center and spreading fluorescence described above. The first evidence for change was the appearance of a ring-shaped fluorescence where the center pixels were dimmer than those in the periphery (Figure 4). The integrated intensity of the structure was greater than that of the granule before the event. Subsequent changes were variable. Some of the rings were stable for one or more seconds (Figure 4, A and C). In others, the center pixels seemed to brighten (Figure 4B, compare 0.2 and 0.3 s). Sometimes the fluorescence would spread beyond the margins of the original ring.

Both the ring-shaped fluorescence and the bright center and spreading fluorescence are apparent in the sequence in Figure 4B. The fusion of a granule by 0.1 s (arrow) resulted in a small fluorescent ring that is still apparent at 0.2 s. A second granule fused by 0.4 s (arrowhead) with its fluorescence immediately spreading without indication of a ring. Thus, these two types of events can occur in proximity at about the same time.

The sudden appearance of a ring together with an increase in fluorescence suggests a fusion event in which the granule membrane retains concavity for at least 200 ms (Figure 5A, c and d). Indeed, quantitative considerations support this conclusion. First, the recessed granule membrane should cause some of the Vamp-GFP to be subjected to lower intensity excitation, resulting in dimmer central pixels, as is observed. Second, although the fluorescence should increase, the relative increase should be less than if the granule completely flattened into the plane of the plasma membrane. This is also the case. The distribution of the relative fluorescence increase upon formation of the ring structure is shifted to lower values compared with the distribution of the bright center and spreading fluorescence events (Figure 5B) The populations were significantly different ($p < 0.006$, Mann-Whitney test). Finally, the images obtained are consistent with computed images of fusion events with retained concavity, as described below.

Modeling of Exocytotic Images

The radii of images of individual granules (appearing as 200- to 300-nm radius diffuse disks) are only a little larger than the optical resolution of the microscope (calculated at 184 nm). To better interpret the images, the expected image patterns of fusion events were simulated by computer (Figure 6) for a fluorescent spherical shell fusing with and spreading into a plane. The spherical area lost to truncation by the plane was deposited in an annulus around the central hole at the truncation. (Diffusion of the Vamp-GFP was not taken into account.) The 2D-projected fluorescence from this structure as would be excited by an evanescent field (decay constant d = 55 nm) was convoluted with an appropriate theoretical Airy disk point spread function (which was also verified experimentally) to provide a simulated image. Examples of the geometries and the simulated images for various truncation depths are presented in Figure 6A. The simulated images demonstrate that, despite the small size of the granules, fusion events in which the granule retains concavity should be detectable with the optics used. The

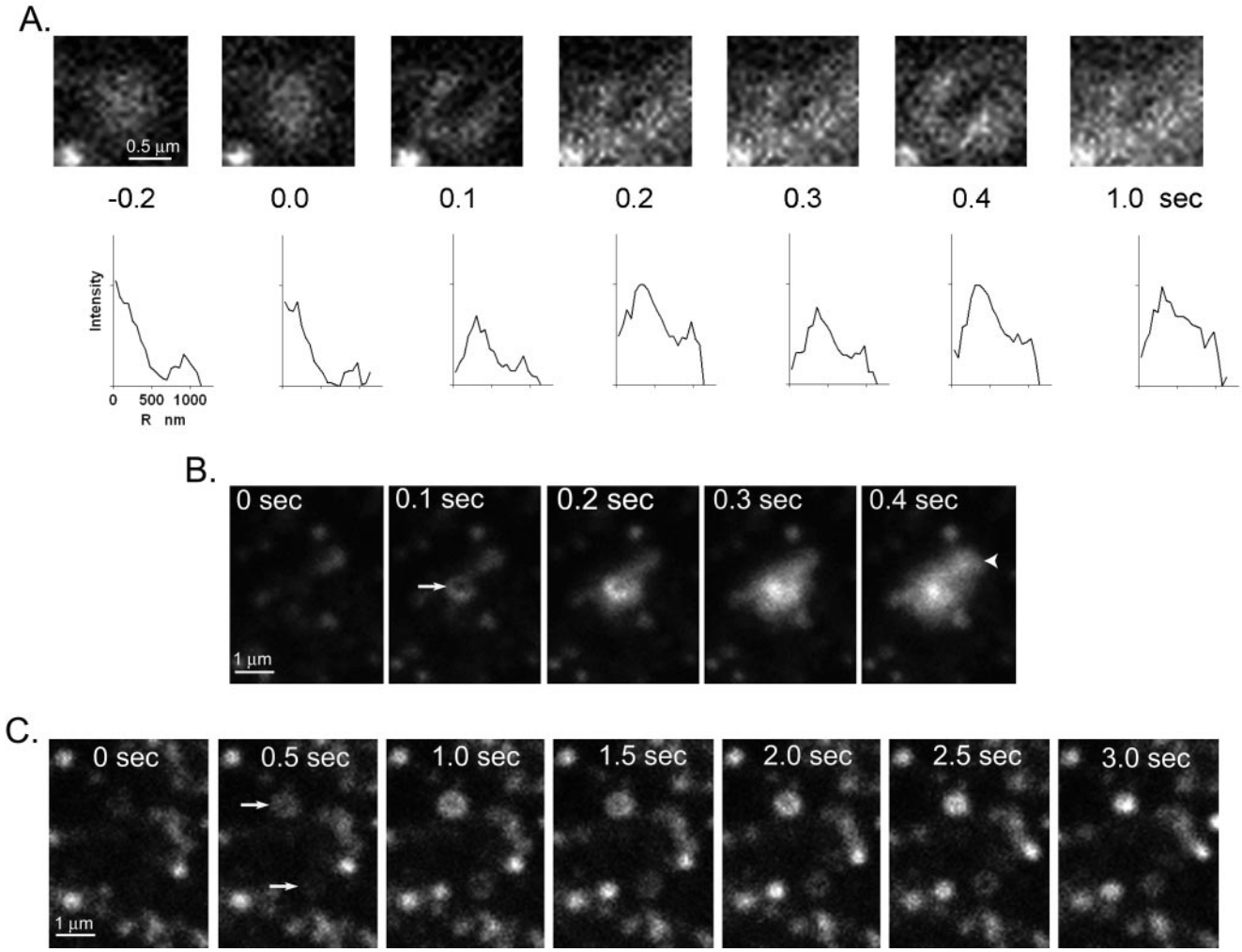

Figure 4. Fusion events in which the center has a lower fluorescence than the surround. (A) Fusion occurred between 0 and 0.1 s. Below each image is the Vamp-GFP intensity (with background subtracted) averaged as a function of radial distance (*r*) away from the granule center. (B) A similar event to that in A occurred by 0.5 s (indicated by arrow) except that the center brighten at 0.3 s, consistent with the granule membrane flattening into the plane of the plasma membrane. Another fusion event occurs between 0.3 and 0.4 s (arrowhead) with bright center pixels. (C) Two fusion events occur between 0 and 0.5 s (arrows) with the centers of each dimmer than the surround. Both of these events were relatively long-lived (~2 s). Note the different scales in B and C compared with A.

apparent recess ($z_{apparent}$; see *Materials and Methods*) generally gives two possible values for the actual recess (z_{actual}) (Figure 6B), with a maximum possible $z_{apparent}$ (82 nm) at a one particular z_{actual} (200 nm). Above this z_{actual}, the dark image of the small fusion pore fills in due to the blurring from off-center fluorescence; below this optimal z_{actual}, even the distal part of the recess is close enough to the plane to be excited significantly by the evanescent field.

For eight events seen in the experiments on chromaffin cells in which rings formed without immediate spreading, $z_{apparent}$ was calculated from the ratio of the dimmest pixel in the center to the brightest pixel in the ring. The average $z_{apparent}$ was 50 ± 9 nm, giving an actual recess z_{actual} of 120 or 240 nm. The three largest $z_{apparent}$ values were ~80 nm, giving a z_{actual} of ~200 nm.

The diameters (at half-maximal intensity) of the simulated images of a granule completely flattened and fused into the plane of the plasma membrane (z_{actual} = 0 nm) and a granule barely touching the membrane (z_{actual} = 300 nm) are 584 and 256 nm, respectively. The ratio of the diameters of the convoluted images of the completely flattened fused granule to the barely touching unfused granule is thereby 2.28. A ratio of 2.0 would have resulted if images were not blurred by the point spread function.

Granule Motion before Exocytosis

The distinct signature of fusion obtained with Vamp-GFP–labeled granules permitted identification of the beginning of the fusion event to within 100 to 200 ms. Individual chromaffin granules in 19 cells were tracked backwards in time from the first frame in which fusion was evident (sudden increase in intensity with simultaneous or subsequent spreading of the fluorescence). Images were taken at 10–14 Hz. There were a variety of behaviors. Most of the granules that fused (152 of 216, 70%) were present in the evanescent field for ~12 s or longer. A small fraction of granules (18 of 216, 8%) were present for greater than 300 ms but less than ~2 s before fusion.

Importantly, a significant number of granules, 46 of 216 (22%), were not detectable in the evanescent field before 300 ms preceding fusion. Some were not evident even 100

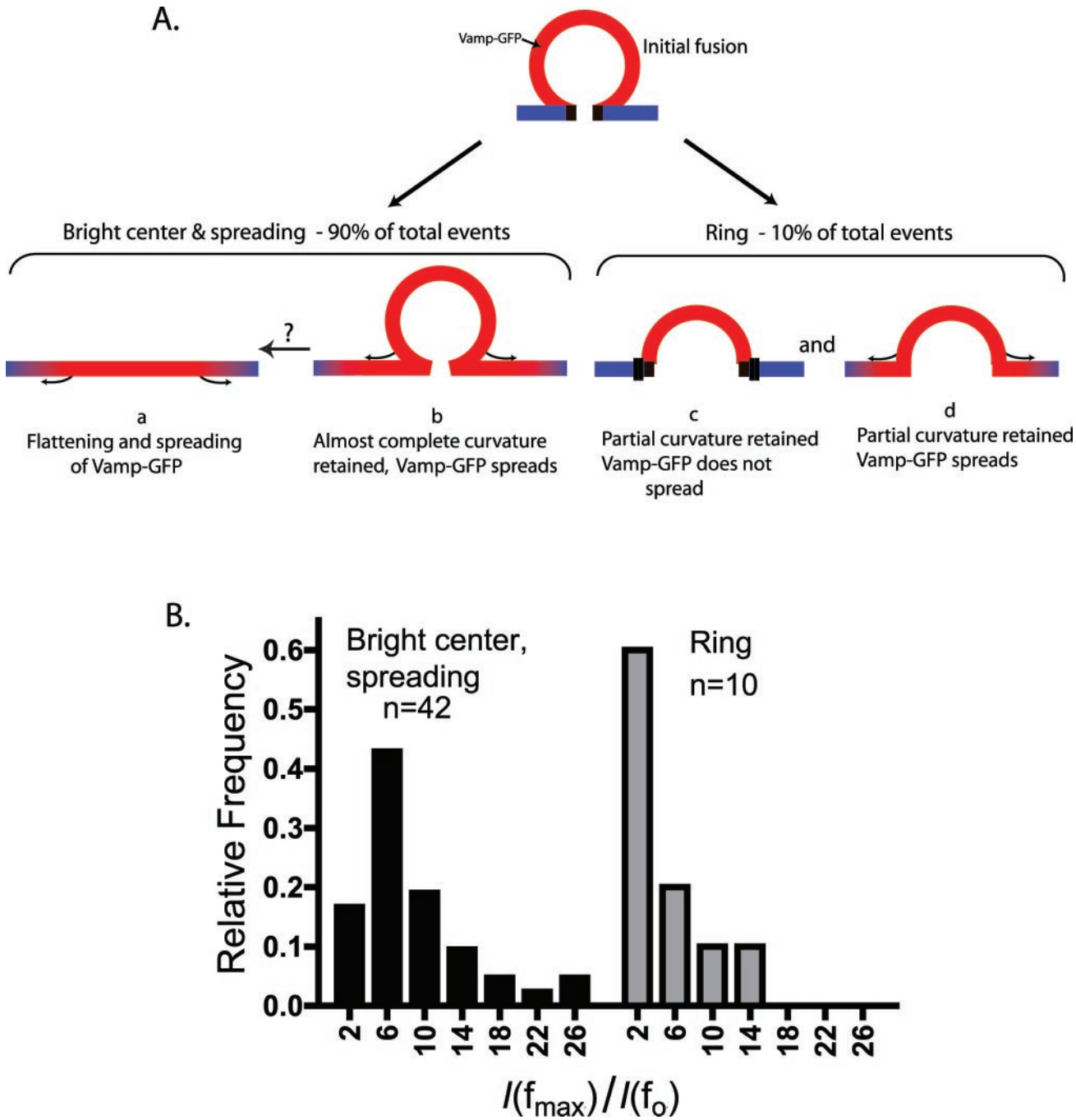

Figure 5. Different types of fusion events. (A) Schematic of possible configurations of a fused chromaffin granule. (B) The distribution of the ratios of maximal integrated intensity observed after fusion in some frame f_{max}, denoted as $I(f_{max})$, to the integrated intensity in the last frame f_0 before fusion, denoted as $I(f_0)$. Distributions are presented for two distinct types of events, the bright center and spreading events observed in 90% of cases, and the ring structures observed 10% of cases. Note that relatively small increases in total intensity characterize the distribution of intensity ratios of ring structures. The populations are significantly different ($p < 0.006$, Mann-Whitney test).

ms before fusion. This behavior could reflect granules that suddenly moved into the evanescent field from deeper within the cell. However, another possibility is that these granules had too little Vamp-GFP to be detected earlier. We, therefore, compared the maximal GFP fluorescence on the plasma membrane from granules that were long-lived in the evanescent field with those that suddenly arrived. We used postfusion Vamp-GFP intensities to assure that comparisons were made at the defined pH of the extracellular medium (pH 7.4). These intensities were likely to be proportional to the amount of Vamp-GFP originally in the granule membrane. The distribution of maximal fluorescence intensities of suddenly appearing granules overlapped with that of granules that were stably present, both in data on individual cells and in data combined from many cells. Only 10% of the granules that were detectable for ~12 s in the evanescent field had intensities after fusion that were greater than the brightest

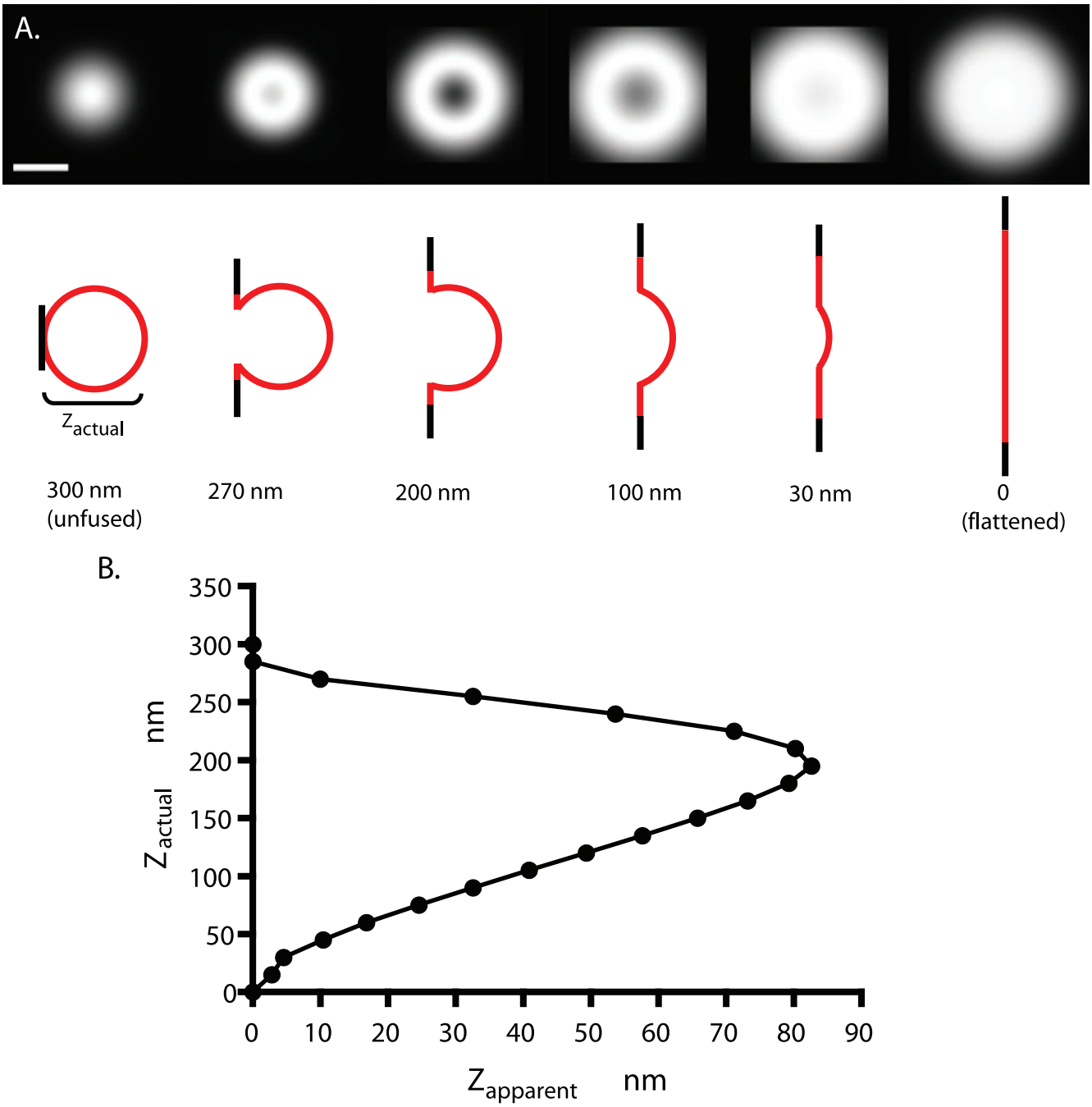

Figure 6. Computed exocytotic images. The image patterns that might be expected with TIRFM optics for different profiles of a spherical granule fusing with a planar plasma membrane were computed (see *Materials and Methods*) assuming a 300-nm initial granule diameter, Vamp-GFP-evenly distributed in the granule membrane at all times, and an evanescent field decay constant of 55 nm. The truncated area flattens into a planar annulus with a central hole at the truncation and an outside radius that conserves the total surface area of the granule. The initial projection was convoluted with a point spread function that was derived theoretically and agrees with an experimentally derived estimate from 20-nm-diameter fluorescent beads. (A) The top images are the computed point spread function convoluted images of the exocytotic profiles schematically depicted below. Bar, 300 nm. (B) Relationship between the actual depth of the recessed granule membrane z_{actual} and the apparent depth $z_{apparent}$, determined by the ratio of the intensities of the dimmest pixel in the center and the brightest in the periphery. Note that for all values of $z_{apparent}$ except the largest, there are two values for z_{actual}. Apparent depth $z_{apparent}$ is greatest when z_{actual} is ~200 nm.

events from granules that appeared within 300 ms of fusion. Thus, most of the granules that suddenly appeared would have been detected if they were present within the evanescent field for longer periods. We conclude that granules that suddenly approached the membrane from beyond the evanescent field, as well as granules that were positioned within the evanescent field for many seconds, were able to undergo exocytosis.

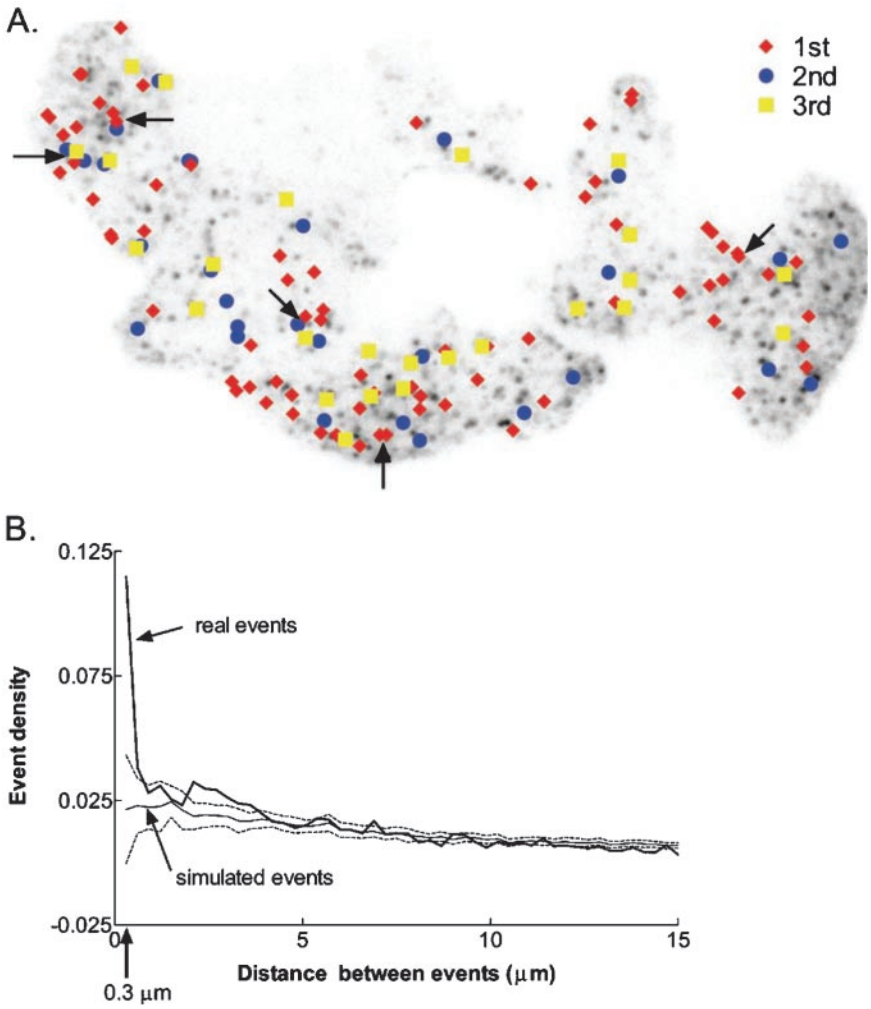

Figure 7. Spatial distribution of exocytotic events in a cell. The cell was stimulated three times for ~5 s with the nicotinic agonist DMPP. There were 3- and 8-min intervals between stimulations. (A) Image of the cell with the locations of fusion events during successive stimulations. Arrows indicate several sites where multiple fusions occurred, either during the same or successive stimulations. (B) Frequency of events at different distances from each other. The distances from each event to all later events in that cell were calculated and then binned in 0.3-μm ranges. The number of events in each bin was divided by the area of the annulus, $\pi(r_2^2 - r_1^2)$, to obtain an event density. Also plotted are the results from 1000 simulated experiments (± SD, dashed lines) of randomly generated events. The simulated cell had the same size and shape as the real cell. An exocytotic site was more likely to have another event occur within 0.3 μm (indicated by arrow on *x*-axis) than can be accounted for by chance.

Microdomains Have Increased Probability of Fusion Events

The spatial distribution of exocytotic events was examined in two cells with a large number of fusion events. One of the cells is shown in Figure 7A. It underwent three rounds of DMPP stimulation separated by 3- and 8-min intervals. (The first stimulation is Supplemental Movie 1.) Arrows indicate several sites where multiple fusions occurred, either during the same or successive stimulations. The tendency of exocytotic sites to be localized was quantified by calculating the distance between events. The frequency distribution of the separation (0.3-μm bin sizes) was normalized by the area of the bin to obtain a frequency density (Figure 7B). We compared these results to those from a set of computer-simulated, randomly generated events in an area of the same shape and size as the experimental cell. The simulation was repeated 1000 times to generate a mean and SE for each separation. The results for the real cell and the simulated cell were not significantly different at separations greater than 0.3 μm. However, an exocytotic site was much more likely to have another event within 0.3 μm than can be accounted for by chance. The actual and computer-simulated number of events that occur within 0.3 μm of another was 28 and 14, respectively. The 14 excess represents 10% of the total of 139 events. Similar results were obtained for the second cell.

DISCUSSION

Fusion Events Imaged by Vamp-GFP

Using TIRFM, we visualized and analyzed fusion events in regulated exocytosis from the point of view of a granule membrane protein, Vamp-GFP. Approximately 90% of the individual events detected upon nicotinic stimulation resulted in a sudden brightening and rapid spreading of the fluorescence into the plane of the plasma membrane. In these events, the center pixels were the brightest at all times after fusion, consistent with diffusion from a small source. If it were not for the optical resolution limit, a granule that partially retains concavity upon fusion would show submaximal central pixels in the TIRFM image. However, because the granules are only a little larger than the resolution of the microscope, the optics may have limited the ability to detect submaximal central intensity. The images were enhanced using several different deconvolution algorithms. Although there was some sharpening of the images, new features did not emerge (unpublished data). Another approach also was used to interpret the events. Simulated image patterns of fusion events in the evanescent field with different possible geometries of fusion were computed, including convolution with a point spread function as indicated by both theory and the actual optics (Figure 6). The results indicated that if the granule partially retained con-

cavity immediately upon fusion, the optics had the capacity to detect submaximal central pixels. Conversely, the analysis indicated that the intensities of central pixels would have been maximal immediately upon fusion if the membrane completely or almost completely flattened. The central pixels also would have been maximal if the fused granule remained almost completely spherical (recess greater than 285 nm for a 300-nm-diameter granule) with subsequent diffusion of Vamp-GFP through a small fusion junction into the plasma membrane. Even in the second possibility, the diameter of the idealized junction of the granule and plasma membrane could be relatively large, 130 nm with a 285-nm recess, compared with the electrophysiologically estimated diameter of the fusion pore, 2–3 nm (Albillos *et al*., 1997). Either interpretation is consistent with electrophysiological experiments that indicate that >90% of fusion events in chromaffin cells normally result in irreversible and large expansion of the fusion pore (Ales *et al*., 1999).

Which of the two possibilities is most likely correct? Both are probably occurring, but in sequence. Transient granule concavity after fusion in chromaffin cells has been suggested by interference reflection microscopy (Llobet *et al*., 2003) and by two-photon excitation imaging by using an extracellular fluorescent probe (Takahashi *et al*., 2002). Lifetimes of ~40 ms were measured (Takahashi *et al*., 2002). Retained granule concavity in PC12 cells has been suggested using TIRFM (Taraska *et al*., 2003). The bright center and spreading fluorescence that we commonly observed probably reflects the rapid progression of an initially fused and spherical granule (Figure 5A, b) that flattens into the plane of the plasma membrane (Figure 5A, a) as the Vamp-GFP simultaneously diffuses through the fusion junction.

Some of the fusion events (~10% of the total events) were qualitatively different from those described above. These events were characterized by the sudden appearance of rings with dimmer central pixels (Figure 4). The quantitative analysis of these events coupled with optical modeling suggests that the rings reflect a significant amount of retained granule membrane concavity after fusion. The modeling suggests that the membrane was recessed ~200 nm, assuming homogeneous distribution of the Vamp-GFP in the granule membrane. Retained granule membrane concavity lasting for seconds to minutes after exocytosis had been observed in pancreatic acinar cells (Schneider *et al*., 1997) and insulin-secreting β cells (Takahashi *et al*., 2002). In the present experiments, the fluorescence usually did not spread rapidly, indicating restricted diffusion of the Vamp-GFP into the plasma membrane (Figure 5A, c). Sometimes the ring persisted for several seconds. In other cases, the structure became smaller and punctate, which may correspond to fast kiss-and-run detected with electrophysiological techniques in chromaffin cells (Ales *et al*., 1999). Fast kiss-and-run is characterized by full catecholamine release but incomplete and reversible fusion pore expansion (average fusion pore lifetime 400 ms) and accounts for 5% of the total fusion events detected electrophysiologically (Albillos *et al*., 1997; Ales *et al*., 1999; Dernick *et al*., 2003).

The two types of fusion events, imaged as either rapid spreading of bright center fluorescence or dim center, ring fluorescence, suggest differences in the fusion junction between the plasma membrane for different exocytotic events or differences in the state of Vamp-GFP in the granule membrane. As discussed below, the rapidly spreading fluorescence indicates that Vamp-GFP is not impeded in its diffusion into the plasma membrane. Ring structures, on the other hand, reflect restricted movement of Vamp-GFP. The restriction could occur because of a diffusion barrier at the fusion junction or because the Vamp-GFP is bound to other components in the granule membrane.

Vamp-GFP Rapidly Diffuses from the Site of Fusion into the Plasma Membrane

For most of the fusion events, the sudden increase in Vamp-GFP fluorescence was accompanied by rapid spreading of the protein into the plane of the plasma membrane with an apparent diffusion coefficient of $2.0 \pm 0.3 \times 10^{-9}$ cm^2/s. Similar results have been obtained for another secretory vesicle membrane protein, VSVG-GFP or VSVG-YFP, in the constitutive secretory pathway (Schmoranzer *et al*., 2000; Toomre *et al*., 2000). VSVG-GFP/YFP spread in the plasma membrane after fusion with an apparent diffusion coefficient of $1.1–1.3 \times 10^{-9}$ cm^2/s. The diffusion coefficient of Vamp-GFP is comparable with the highest diffusion coefficients for proteins in cell membranes (e.g., 4×10^{-9} for rhodopsin) (Jacobson *et al*., 2003). Thus, transiently expressed Vamp-GFP was usually not obstructed in its movement from the granule membrane to the plasma membrane. The width of the punctate fluorescence doubled in 200–300 ms, which is similar to the time frame for attaining maximal fluorescence (~200 ms). The spreading is slower than the average fusion pore lifetime that has been measured electrophysiologically (~20 ms) (Dernick *et al*., 2003), and therefore likely occurred after rather than during fusion. However, it should be noted that the high temporal resolution fusion pore data were obtained in patch-clamp experiments in which the plasma membrane was under lateral stress, which could quicken the opening of the fusion pore.

The extensive spreading of Vamp-GFP in the plasma membrane is not a general characteristic of granule membrane proteins. Dopamine-β-hydroxylase, an endogenous granule membrane marker, remains punctate in the plasma membrane after fusion when visualized by immunocytochemistry (Wick *et al*., 1997). GFP-phogrin, which labels the membrane of large dense core granules, also remains punctate upon granule fusion in PC12 cells (Taraska *et al*., 2003) and insulinoma cells (Tsuboi *et al*., 2000) visualized with TIRFM. However, CDC63-GFP, a lysosomal membrane protein does spread in the plasma membrane after exocytosis (Jaiswal *et al*., 2002). The different behaviors probably reflect differences in the proteins themselves and/or their interactions with granule components.

It has recently been reported that a small lipid-like molecule diffuses from the secretory granule membrane into the plasma membrane upon exocytosis (Taraska and Almers, 2004). Prolonged incubation of PC12 cells with a fluorescent, lipophilic probe, FM4-64, labels the inner leaflet of large dense core granules in PC12 cells. The dye is rapidly released upon exocytosis. The kinetics of the response reflects both diffusion in and desorption from the plasma membrane and suggests that lipids as well as proteins can diffuse from the granule to the plasma membrane.

SNARE Complex Formation Leading to Exocytosis Occurs within Several Hundred Milliseconds

Approximately 20% of the granules that underwent fusion were present in the evanescent field for <300 ms, with some becoming apparent only upon fusion. For those granules that suddenly occurred, the interaction of the granule with the plasma membrane that leads to exocytosis must have occurred within 100–300 ms of fusion. These observations suggest that interactions of granule membrane and plasma membrane proteins important for exocytosis can be rapid.

Preferred Domains for Exocytosis

A statistical analysis of the spatial distribution of exocytotic events in individual cells indicated that an exocytotic site was more likely to have another event within 0.3 μm than could be accounted for by chance (Figure 7). In contrast, the distribution of events separated by 0.6 μm or greater was random. The increased tendency for proximity of events accounts for 10% of the total. These events may reflect infrequent instances of sequential exocytosis in which granules fuse with a granule that has previously fused with the plasma membrane. Sequential exocytosis is a major characteristic of fusion in pancreatic acinar cells (Nemoto *et al*., 2001), eosinophils (Scepek and Lindau, 1993; Hafez *et al*., 2003), pituitary lactotrophs (Cochilla *et al*., 2000), and mast cells (Alvarez de Toledo and Fernandez, 1990), but it has not been described in chromaffin cells. Alternatively, they may reflect 0.35-μm-diameter microdomains of elevated Ca^{2+} (40-ms duration), which have recently been observed in chromaffin cells during elevated K^+-induced depolarization (Becherer *et al*., 2003). These sites may have a greater tendency to support exocytosis. (The temporal stability of the localization of the Ca^{2+}microdomains was not reported.)

Similarities of Fusion in the Regulated and Constitutive Pathways Revealed by TIRFM

Post-Golgi transport containers (TCs) have heterogeneous morphologies, including vesicular and tubular structures. The signature of exocytosis of chromaffin granules given by brightening and spreading of Vamp-GFP is similar to that for small vesicles in the constitutive pathway labeled with a fluorescent viral membrane marker VSVG-GFP/YFP (Schmoranzer *et al*., 2000; Toomre *et al*., 2000). For both, there is a manyfold increase in total fluorescence accompanied by free diffusion of the proteins in the plasma membrane. The similarities upon fusion occur despite the different membrane proteins. Remarkably, even the prefusion dynamics of chromaffin granules and TCs are similar. Some TCs occur suddenly in the evanescent field and fuse but many others approach and remain in the evanescent field for minutes before either fusing or moving back into the cell.

There are, of course, important differences in the pathways. The lifetime of TCs in the constitutive pathway is short (minutes) compared with that of chromaffin granules in the regulated pathway (days), and constitutive exocytosis does not require a signal, whereas regulated exocytosis is triggered by elevated Ca^{2+}. The specific proteins involved in the late steps in the two pathways are also distinct. Some are homologous (the SNAREs) but some are highly specific (e.g., synaptotagmin in the regulated pathway). Nevertheless, the similar quantitative descriptions of the final moments of regulated secretory granules and constitutive vesicles are likely to reflect basic similarities of the fusion events in the two pathways.

ACKNOWLEDGMENTS

We thank Dr. Mary A. Bittner many helpful discussion and the reading of the manuscript. This work was funded by a National Institutes of Health grant R01-NS38129 (to D.A.) and a Michigan Economic Development Corporation and the Michigan Life Sciences Corridor grant (to R.W.H.).

REFERENCES

Albillos, A., Dernick, G., Horstmann, H., Almers, W., Alvarez de Toledo, G., and Lindau, M. (1997). The exocytotic event in chromaffin cells revealed by patch amperometry. Nature *389*, 509–512.

Ales, E., Tabares, L., Poyato, J.M., Valero, V., Lindau, M., and Alvarez de Toledo, G. (1999). High calcium concentrations shift the mode of exocytosis to the kiss-and-run mechanism.[comment]. Nat. Cell Biol. *1*, 40–44.

Alvarez de Toledo, G., and Fernandez, J.M. (1990). Compound versus multigranular exocytosis in peritineal mast cells. J. Gen. Physiol. *95*, 397–409.

Axelrod, D. (1981). Cell-substrate contacts illuminated by total internal reflection fluorescence. J. Cell Biol. *89*, 141–145.

Axelrod, D. (2001). Selective imaging of surface fluorescence with very high aperture microscope objectives. J. Biomed. Optics *6*, 6–13.

Axelrod, D. (2003). Total internal reflection fluorescence microscopy in cell biology. Methods Enzymol. *361*, 1–33.

Becherer, U., Moser, T., Stuhmer, W., and Oheim, M. (2003). Calcium regulates exocytosis at the level of single vesicles. Nat. Neurosci. *6*, 846–853.

Breckenridge, L.J., and Almers, W. (1987). Final steps in exocytosis observed in a cell with giant secretory granules. Proc. Natl. Acad. Sci. USA *84*, 1945–1949.

Burke, N.V., Han, W., Li, D., Takimoto, K., Watkins, S.C., and Levitan, E.S. (1997). Neuronal peptide release is limited by secretory granule mobility. Neuron *19*, 1095–1102.

Cochilla, A.J., Angleson, J.K., and Betz, W.J. (2000). Differential regulation of granule-to-granule and granule-to-plasma membrane fusion during secretion from rat pituitary lactotrophs. J. Cell Biol. *150*, 839–848.

Dernick, G., Alvarez, D., and Lindau, M. (2003). Exocytosis of single chromaffin granules in cell-free inside-out membrane patches.[published correction appears in Nat. Cell Biol. 2003: 5, 488]. Nat. Cell Biol. *5*, 358–362.

Duncan, R.R., Greaves, J., Wiegand, U.K., Matskevich, I., Bodammer, G., Apps, D.K., Shipston, M.J., and Chow, R.H. (2003). Functional and spatial segregation of secretory vesicle pools according to vesicle age. Nature *422*, 176–180.

Hafez, I., Stolpe, A., and Lindau, M. (2003). Compound exocytosis and cumulative fusion in eosinophils. J. Biol. Chem. *278*, 44921–44928.

Han, W., Ng, Y.K., Axelrod, D., and Levitan, E.S. (1999). Neuropeptide release by efficient recruitment of diffusing cytoplasmic secretory vesicles. Proc. Natl. Acad. Sci. USA *96*, 14577–14582.

Jacobson, K., Ishihara, A., and Inman, R. (2003). Lateral diffusion of proteins in membranes. Annu. Rev. Physiol. *49*, 163–175.

Jaiswal, J.K., Andrews, N.W., and Simon, S.M. (2002). Membrane proximal lysosomes are the major vesicles responsible for calcium-dependent exocytosis in nonsecretory cells. J. Cell Biol. *159*, 625–635.

Johns, L.M., Levitan, E.S., Shelden, E.S., Holz, R.W., and Axelrod, D. (2001). Restriction of secretory granule motion near the plasma membrane of chromaffin cells. J. Cell Biol. *153*, 177–190.

Llobet, A., Beaumont, V., and Lagnado, L. (2003). Real-time measurement of exocytosis and endocytosis using interference of light. Neuron *40*, 1075–1086.

Nemoto, T., Kimura, R., Ito, K., Tachikawa, A., Miyashita, Y., Iino, M., and Kasai, H. (2001). Sequential-replenishment mechanism of exocytosis in pancreatic acini. Nat. Cell Biol. *3*, 253–258.

Ng, Y.K., Lu, X., Watkins, S.C., Ellis-Davies, G.C.R., and Levitan, E.S. (2002). Nerve growth factor-induced differentiation changes the cellular organization of regulated peptide release by PC12 cells. J. Neurosci. *22*, 3890

Ohara-Imaizumi, M., Nakamichi, Y., Tanaka, T., Ishida, H., and Nagamatsu, S. (2002). Imaging exocytosis of single insulin secretory granules with evanescent wave microscopy. distinct behavior of granule motion in biphasic insulin release. J. Biol. Chem. *277*, 3805–3808.

Oheim, M., Loerke, D., Stuhmer, W., and Chow, R.H. (1998). The last few milliseconds in the life of a secretory granule. Docking, dynamics and fusion visualized by total internal reflection fluorescence microscopy (TIRFM). Eur. J. Biophys. *27*, 83–98.

Oheim, M., and Stuhmer, W. (2000). Tracking chromaffin granules on their way through the actin cortex. Eur. J. Biophys. *29*, 67–89.

Rettig, J., and Neher, E. (2002). Emerging roles of presynaptic proteins in Ca++-triggered exocytosis. Science *298*, 781

Scepek, S., and Lindau, M. (1993). Focal exocytosis by eosinophils–compound exocytosis and cumulative fusion. EMBO J. *12*, 1811–1817.

Schmoranzer, J., Goulian, M., Axelrod, D., and Simon, S.M. (2000). Imaging constitutive exocytosis with total internal reflection fluorescence microscopy. J. Cell Biol. *149*, 23–32.

Schneider, S., Sritharan, K., Geibel, J., Oberleithner, H., and Jena, B. (1997). Surface dynamics in living acinar cells imaged by atomic force microscopy: identification of plasma membrane structures involved in exocytosis. Proc. Natl. Acad. Sci. USA *94*, 316–321.

Steyer, J.A., Horstman, H., and Almers, W. (1997). Transport, docking and exocytosis of single secretory granules in live chromaffin cells. Nature *388*, 474–478.

Stout, A.L., and Axelrod, D. (1989). Evanescent field excitation of fluorescence by epi-illumination microscopy. Appl. Opt. *28*, 5237–5242.

Takahashi, N., Kishimoto, T., Nemoto, T., Kadowaki, T., and Kasai, H. (2002). Fusion pore dynamics and insulin granule exocytosis in the pancreatic islet. Science *297*, 1349–1352.

Taraska, J.W., and Almers, W. (2004). Bilayers merge even when exocytosis is transient. Proc. Natl. Acad. Sci. USA *101*, 8780–8785.

Taraska, J.W., Perrais, D., Ohara-Imaizumi, M., Nagamatsu, S., and Almers, W. (2003). Secretory granules are recaptured largely intact after stimulated exocytosis in cultured endocrine cells. Proc. Natl. Acad. Sci. USA *100*, 2070–2075.

Toomre, D., Steyer, J.A., Keller, P., Almers, W., and Simons, K. (2000). Fusion of constitutive membrane traffic with the cell surface observed by evanescent wave microscopy. J. Cell Biol. *149*, 33–40.

Tsuboi, T., Zhao, C., Terakawa, S., and Rutter, G.A. (2000). Simultaneous evanescent wave imaging of insulin vesicle membrane and cargo during a single exocytotic event. Curr. Biol. *10*, 1307–1310.

Voets, T. (2000). Dissection of three Ca2+-dependent steps leading to secretion in chromaffin cells from mouse adrenal slices. Neuron *28*, 537–545.

Wick, P.W., Senter, R.A., Parsels, L.A., and Holz, R.W. (1993). Transient transfection studies of secretion in bovine chromaffin cells and PC12 cells: generation of kainate-sensitive chromaffin cells. J. Biol. Chem. *268*, 10983–10989.

Wick, P.W., Trenkle, J.M., and Holz, R.W. (1997). Punctate appearance of dopamine-β-hydroxylase on the chromaffin cell surface refects the fusion of individual chromaffin granules upon exocytosis. Neuroscience *80*, 847–860.

Wilson, S.P., Liu, F., Wilson, R.E., and Housley, P.R. (1996). Optimization of calcium phosphate transfection for bovine chromaffin cells: relationship to calcium phosphate precipitate formation. Anal. Biochem. *226*, 212–220.

Zimmerberg, J., Curran, M., Cohen, F.S., and Brodwick, M. (1987). Simultaneous electrical and optical measurements show that membrane fusion precedes secretory granule swelling during exocytosis of beige mouse mast cells. Proc. Natl. Acad. Sci. USA *84*, 1585–1589.